Research Square

Preprints are preliminary reports that have not undergone peer review.
They should not be considered conclusive, used to inform clinical practice,
or referenced by the media as validated information.

A broadly cross-reactive i-body to AMA1 potently inhibits blood and liver stages of Plasmodium parasites

Michael Foley (m.foley@latrobe.edu.au)
La Trobe University
Dimuthu Angage
La Trobe University https://orcid.org/0009-0009-4776-487X
Robin Anders
La Trobe University
Jill Chmielewski
Adelaide University
Janesha Maddumage
La Trobe University
Eva Hesping
The Walter and Eliza Hall Institute of Medical Research,
Sabrina Caiazzo
Walter and Eliza Hall Institute of Medical Research
Keng Heng Lai
Adelaide University https://orcid.org/0000-0002-2111-0466
Lee Yeoh
Burnet Institute https://orcid.org/0000-0001-7872-762X
Herbert Opi
Burnet Institute https://orcid.org/0000-0002-4589-4365
Callum Cairns
La Trobe University
James Beeson
Burnet Institute https://orcid.org/0000-0002-1018-7898
Marc Kvansakul
La Trobe University https://orcid.org/0000-0003-2639-2498
Danny Wilson
University of Adelaide https://orcid.org/0000-0002-5073-1405
Justin Boddey
Walter and Eliza Hall Institute of Medical Research https://orcid.org/0000-0001-7322-2040

Article

Keywords: Plasmodium, AMA1, phage display, i-bodies, invasion inhibition

Posted Date: December 18th, 2023

DOI: https://doi.org/10.21203/rs.3.rs-3671797/v1

License: This work is licensed under a Creative Commons Attribution 4.0 International License.
Read Full License

Additional Declarations: There is **NO** Competing Interest.

A broadly cross-reactive i-body to AMA1 potently inhibits blood and liver stages of *Plasmodium* parasites

Dimuthu Angage[1], Jill Chmielewski[2], Janesha Maddumage[1], Eva Hesping[3,4], Sabrina Caiazzo[3,4], Keng Heng Lai[2], Lee Ming Yeoh[5,6], D. Herbert Opi[5,6], Callum Cairns[1], James Beeson[5,8], Marc Kvansakul[1], Justin A. Boddey[3,4], Danny Wilson[2,5,7], Robin F. Anders[1] & Michael Foley[1,9]

[1]Department of Biochemistry and Chemistry, La Trobe Institute for Molecular Sciences, La Trobe University, Victoria, Australia 3086

[2]Research Centre for Infectious Diseases, School of Biological Sciences, The University of Adelaide, South Australia, Australia 5005

[3]Infectious Diseases & Immune Defense Division, The Walter and Eliza Hall Institute of Medical Research, 1G Royal Parade, Parkville, Victoria, Australia 3052

[4]Department of Medical Biology, The University of Melbourne, Parkville, Victoria, Australia 3052

[5]Burnet Institute, Melbourne, Victoria, Australia 3004

[6]Department of Medicine, The University of Melbourne, Parkville, Victoria, Australia 3052

[7]Institute for Photonics and Advanced Sensing (IPAS), University of Adelaide, South Australia, Australia 5005

[7]Central Clinical School and Department of Microbiology, Monash University, Clayton, Victoria, Australia 3800

[9]AdAlta, 15/2 Park Drive, Bundoora, Victoria, Australia 3083

Keywords- *Plasmodium*, AMA1, phage display, i-bodies, invasion inhibition

Abstract

Broadly cross-reactive anti-malarial vaccines and therapeutic interventions are needed to achieve better outcomes in controlling and, eventually, eradicating malaria. Apical membrane antigen-1 (AMA1) is a structurally and functionally conserved malarial vaccine candidate involved in the tight junction formation with the rhoptry neck protein (RON) complex at the host cell-parasite interface. This interaction is crucial for all *Plasmodium* parasites to invade human erythrocytes, hepatocytes and mosquito salivary glands effectively. However, extensive surface polymorphisms have induced *P. falciparum* strain-specific protection which has so far hindered the progression of AMA1-based interventions beyond the first clinical trial. Here, we identified a humanised single-domain (i-body) that recognises a conserved pan-species conformational epitope in AMA1 with low nanomolar affinity and inhibits the binding of the RON2 ligand to AMA1. Structural characterisation indicated that the WD34 i-body epitope engages the centre of the conserved hydrophobic cleft in AMA1, where interacting residues are highly conserved among all *Plasmodium* species and other apicomplexans. Further, we

showed that WD34 inhibits merozoite invasion into RBCs by multiple *Plasmodium* species and hepatocyte invasion by *P. falciparum* sporozoites. Our work describes the identification of the first pan-species AMA1 biologic with high multi-lifecycle stage invasion inhibitory activity. This work identifies new tools for species-independent immunoprophylaxis and a possible target for structure-based vaccine development against malaria.

Main/ Introduction

Invasion of erythrocytes by *Plasmodium* merozoites initiates all the clinical manifestations of malaria[1]. The invasion process is fast, sequential, and tightly regulated by multiple interactions between parasite ligands and receptors on the erythrocyte surface[2,3]. Following attachment to the erythrocyte membrane, the merozoite reorientates, allowing the apical end to form a tight junction as an entry point for invading host erythrocytes[4]. Parasite antigens involved in this attachment and invasion process have been explored as potential anti-malarial blood-stage vaccines and therapeutic targets[5-7].

AMA1 is a micronemal protein released onto the parasite surface following the attachment of the merozoite to the erythrocyte membrane. AMA1 subsequently binds to the ectodomain of the RON2 protein on the erythrocyte surface to form a tight gap junction [8-10]. There is considerable experimental evidence that the AMA1-RON2 complex is also involved in sporozoite invasion of mosquito salivary glands and mammalian hepatocytes, [11-13]. Previously, AMA1 was considered a leading vaccine candidate due to its relative structural conservation and pivotal role in host cell invasion by multiple stages of the parasite life cycle[3,14]. However, polymorphisms in AMA1 induce strain-specific protection, and for this reason, clinical development of AMA1 has been halted[15-19]. Numerous attempts were made to generate cross-reactive anti-AMA1 antibodies to overcome the antigenic diversity[20-22]. Even though a few cross-reactive monoclonal antibodies were generated against AMA1, these antibodies lacked functional activity[23,24].

i-bodies are fully human single-domain immunoglobulins inspired by the structural features of the shark variable new antigen receptor (V_{NAR}) designed to overcome the limitations of conventional monoclonal antibodies[25]. The i-body consists of a human scaffold (first Ig domain of the human neural cell adhesion molecule) and two complementarity determining regions (CDR) 1 & 3 where they would exist in the V_{NAR} [25]. By randomizing sequences of CDR1 (fixed length) and CDR3 (variable length), a library of over 10^{10} unique i-bodies was generated. Due to their smaller size compared to conventional antibodies and easy access to cryptic epitopes, i-bodies have been considered as potential therapeutics against numerous diseases, including osteoporosis, idiopathic pulmonary fibrosis, and renal fibrosis[25-27]. Therefore, we hypothesised that selecting i-bodies against *Pf*AMA1 could identify functionally conserved epitopes that have not been previously recognised.

In this study, we used phage display to identify a novel i-body, WD34, which binds to AMA1 in multiple *Plasmodium* species with low nanomolar affinity. By determining the crystal structure of WD34:AMA1 complexes, we have defined the binding footprint of WD34. Using several *Plasmodium* strains and species, we demonstrated the inhibitory role of WD34 in merozoite and sporozoite invasion. Our findings identify WD34 as the first pan-species antimalarial antibody with high invasion inhibitory activity.

Results

Identification of strain transcending i-body binders to AMA1

The single domain i-body library, described by Griffiths, et al. [25] was biopanned on recombinant AMA1 (recAMA1) of two *P. falciparum* strains, 3D7 and W2mef. These two isoforms of AMA1 were chosen because they differ at many of the polymorphic sites in the antigen[28]. In addition to panning on individual *Pf*AMA1 isoforms, a cross-panning strategy was employed in which phage selected after three rounds of panning on one AMA1 isoform were subjected to three further panning rounds on the other isoform (Fig. 1a).

Enrichment of phage expressing i-bodies binding to recAMA1 was observed after three rounds of panning on either the 3D7 or W2mef antigen (Fig. 1b, c). These phage pools contained i-bodies that bound to AMA1 of other *P. falciparum* strains (7G8, FVO, HB3 and D10), indicating that the pools contained phage that expressed i-bodies with broad specificity (Extended data Fig. 1-2). The three rounds after cross-panning showed evidence of binders to both the 3D7 and W2mef isoforms of recAMA1, which were used in the original panning campaign. Since these ELISAs were carried out using pooled phage, it was possible that the pools contained many clones that bound to one or other, but not both forms of recAMA1. However, analysis by ELISA identified several clones from both campaign pools that bound to both 3D7 and W2mef recAMA1. ELISA screening of 48 clones from the last round of each panning campaign revealed a wide spectrum of binding to the different forms of AMA1. This presumably reflected the level of i-body expression in addition to the binding affinity for a particular form of AMA1 (Fig. 1d). Sanger sequencing of 117 of these positive clones from all panning campaigns identified 12 unique i-body sequences (Fig. 1e).

When twelve i-bodies representing these sequences were tested for their ability to bind to a range of *Pf* recAMA1 isoforms (3D7, W2mef, 7G8, FVO, D10, and HB3) different binding specificities were observed (Fig. 1f). WD33 and WD34 i-bodies bound to all AMA1 isoforms examined, but not to reduced and alkylated AMA1, indicating that these two i-bodies bind to conserved conformational epitopes in *Pf*AMA1 (Fig. 1g). Notably, i-bodies with the WD33 and WD34 sequences were identified exclusively in the cross-panning campaign (Extended Fig. 3).

Fig. 1 AMA1 specific i-body selection and identification. a. Graphical description of **the** biopanning strategy of phage-displayed i-body library against 3D7 and W2mef AMA1. **b.** ELISA of phage pools from the biopanning campaign against immobilised 3D7 AMA1. **c.** ELISA of phage pools from the biopanning campaign against immobilised W2mef AMA1. In both campaigns, three replicates were performed. Error bars represent standard deviation. DR0-6 represents direct panning rounds, and CPR1-3 represents cross-panning rounds. **d.** Single clone i-body screening for AMA1 binding. Forty-eight clones were randomly selected from each biopanning campaign. Small-scale i-body expression in *E. coli* of each clone was performed and assessed for AMA1 binding as 1:2 dilution in PBS using ELISA. The binding of the i-bodies to the different AMA1 molecules is represented as a heat map. **e.** Sequence alignment of AMA1-specific i-bodies with the CDR1 and CDR3 sequences highlighted in blue. **f.** Binding profile of i-bodies against recombinant *Pf*3D7, W2mef, 7G8, FVO, HB3, D10 AMA1 isoforms and reduced and alkylated 3D7 AMA1 represented as a heat map where the darker the shade, the greater the binding. Each i-body was tested in triplicate. **g.** Binding analysis of AMA1 conformational epitope-specific WD33 and WD34 i-bodies with *Pv* and *Pc*AMA1. Three replicates were performed, and error bars represent the standard deviation.

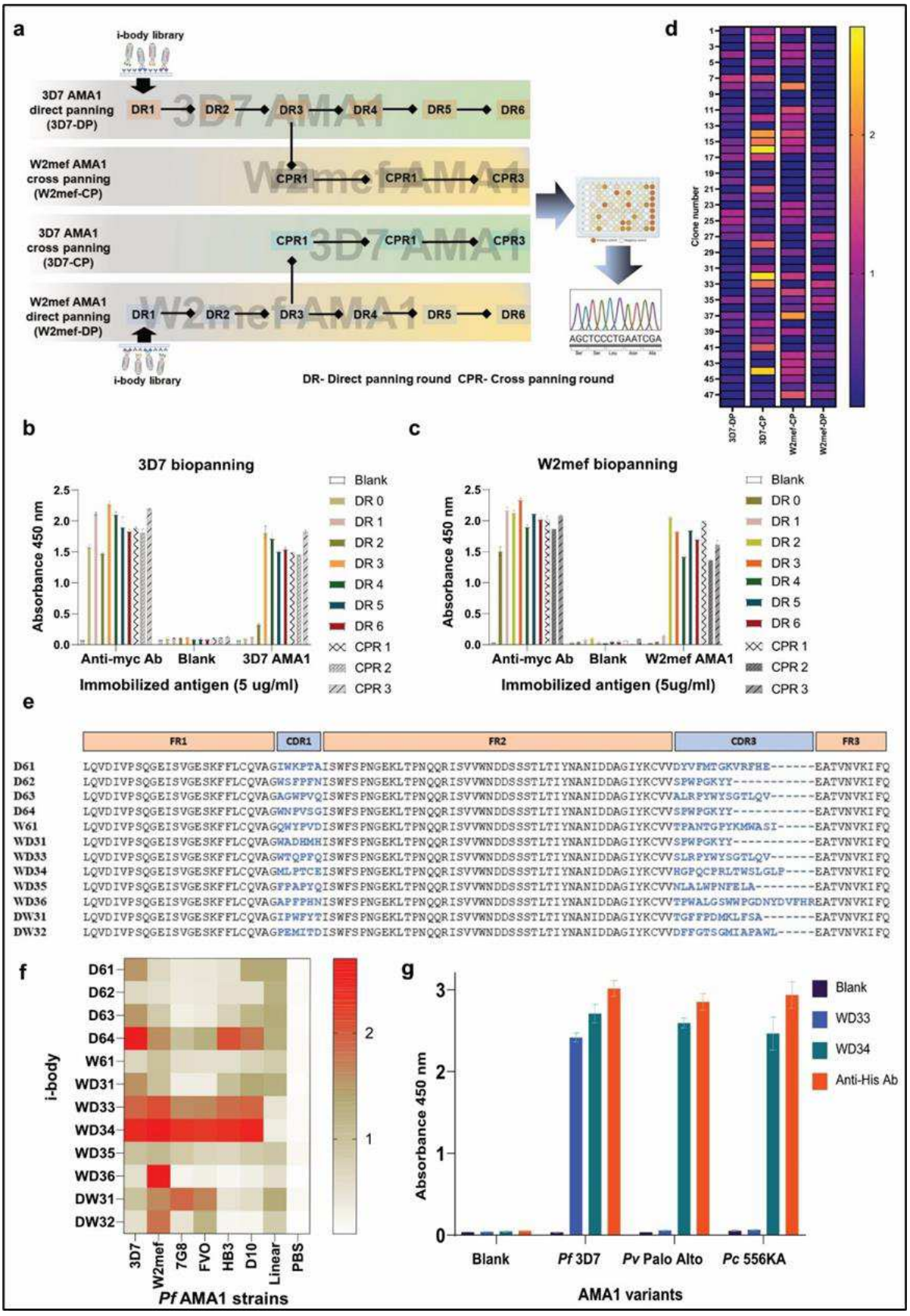
a
i-body library
3D7 AMA1 direct panning (3D7-DP)
DR1
DR2
DR3
DR4
DR5
DR6
3D7 AMA1
W2mef AMA1 cross panning (W2mef-CP)
CPR1
CPR3
W2mef AMA1
3D7 AMA1 cross panning (3D7-CP)
W2mef AMA1 direct panning (W2mef-DP)
i-body library
AGCTCCCTGAATCGA
DR- Direct panning round CPR- Cross panning round
d
Clone number
3D7-DP
3D7-CP
W2mef-CP
W2mef-DP
b
3D7 biopanning
Absorbance 450 nm
Anti-myc Ab
Blank
3D7 AMA1
Immobilized antigen (5 ug/ml)
Blank
DR 0
DR 1
DR 2
DR 3
DR 4
DR 5
DR 6
CPR 1
CPR 2
CPR 3
c
W2mef biopanning
Absorbance 450 nm
Anti-myc Ab
Blank
W2mef AMA1
Immobilized antigen (5ug/ml)
e
FR1
CDR1
FR2
CDR3
FR3
D61 LQVDIVPSQGEISVGESKFFLCQVAGIWKPTAISWFSPNGEKLTPNQQRISVVWNDDSSSTLTIYNANIDDAGIYKCVVDYVFMTGKVRFHE------EATVNVKIFQ
D62 LQVDIVPSQGEISVGESKFFLCQVAGWSFPFNISWFSPNGEKLTPNQQRISVVWNDDSSSTLTIYNANIDDAGIYKCVVSPWPGKYY----------EATVNVKIFQ
D63 LQVDIVPSQGEISVGESKFFLCQVAGAGWFVQISWFSPNGEKLTPNQQRISVVWNDDSSSTLTIYNANIDDAGIYKCVVALRPYWYSGTLQV------EATVNVKIFQ
D64 LQVDIVPSQGEISVGESKFFLCQVAGWNFVSGISWFSPNGEKLTPNQQRISVVWNDDSSSTLTIYNANIDDAGIYKCVVSPWPGKYY----------EATVNVKIFQ
W61 LQVDIVPSQGEISVGESKFFLCQVAGQWYPVDISWFSPNGEKLTPNQQRISVVWNDDSSSTLTIYNANIDDAGIYKCVVTPANTGPYKMWASI-----EATVNVKIFQ
WD31 LQVDIVPSQGEISVGESKFFLCQVAGWADHMHISWFSPNGEKLTPNQQRISVVWNDDSSSTLTIYNANIDDAGIYKCVVSPWPGKYY----------EATVNVKIFQ
WD33 LQVDIVPSQGEISVGESKFFLCQVAGWTQPFQISWFSPNGEKLTPNQQRISVVWNDDSSSTLTIYNANIDDAGIYKCVVSLRPYWYSGTLQV------EATVNVKIFQ
WD34 LQVDIVPSQGEISVGESKFFLCQVAGMLPTCEISWFSPNGEKLTPNQQRISVVWNDDSSSTLTIYNANIDDAGIYKCVVHGPQCPRLTWSLGLP----EATVNVKIFQ
WD35 LQVDIVPSQGEISVGESKFFLCQVAGFPAPYQISWFSPNGEKLTPNQQRISVVWNDDSSSTLTIYNANIDDAGIYKCVVNLALWPNFELA--------EATVNVKIFQ
WD36 LQVDIVPSQGEISVGESKFFLCQVAGAPFPHNISWFSPNGEKLTPNQQRISVVWNDDSSSTLTIYNANIDDAGIYKCVVTPWALGSWWPGDNYDVFHREATVNVKIFQ
DW31 LQVDIVPSQGEISVGESKFFLCQVAGIPWFYTISWFSPNGEKLTPNQQRISVVWNDDSSSTLTIYNANIDDAGIYKCVVTGFFPDMKLFSA-------EATVNVKIFQ
DW32 LQVDIVPSQGEISVGESKFFLCQVAGPEMITDISWFSPNGEKLTPNQQRISVVWNDDSSSTLTIYNANIDDAGIYKCVVDFFGTSGMIAPAWL-----EATVNVKIFQ
f
i-body
D61
D62
D63
D64
W61
WD31
WD33
WD34
WD35
WD36
DW31
DW32
3D7
W2mef
7G8
FVO
HB3
D10
Linear
PBS
Pf AMA1 strains
g
Absorbance 450 nm
Blank
WD33
WD34
Anti-His Ab
Blank
Pf 3D7
Pv Palo Alto
Pc 556KA
AMA1 variants

WD33 and WD34 i-bodies bound to parasite AMA1 under non reducing, but not reducing conditions when used to immunoblot extracts of saponin-lysed late-stage 3D7, W2mef, FVO and 7G8 schizonts expressing different variants of AMA1 (Fig. 2a). Both WD33 and WD34 bound specifically to a band of the predicted size for full-length AMA1 of all AMA1 variants and another band corresponding to a processed fragment of AMA1. The identity of both bands was confirmed using well-characterised anti-AMA1 monoclonal antibodies (Extended data Fig. 4-5). The ability of these i-bodies to bind parasite AMA1 was confirmed by indirect immunofluorescence microscopy, which showed both WD33 and WD34 binding to late schizonts with the expected staining pattern for AMA1, and colocalizing with mAb 5G8, an AMA1 pro-domain specific monoclonal antibody (Fig. 2b).

WD34 binds to the conserved hydrophobic cleft region of AMA1 with low nanomolar affinity

The ability of anti-AMA1 i-bodies to inhibit the interaction of *Pf*RON2 with *Pf*AMA1 was examined using a biotin-tagged RON2 synthetic peptide[10,29]. Initial screening revealed a dramatic reduction of RON2 peptide binding to 3D7 recAMA1 in the presence of an equivalent concentration of WD34 (Fig. 3a). The results of a competition ELISA confirmed that WD34 inhibited the binding of the RON2 peptide to AMA1 in a dose-dependent manner (Fig. 3b). None of the other eleven representative i-bodies tested, including WD33, inhibited the interaction of recAMA1 and the RON2 peptide, further confirming that the WD33 and WD34 epitopes differ. The binding of the WD33 and WD34 i-bodies to different isoforms of *Pf*AMA1 was characterised by surface plasmon resonance (SPR). WD34 bound to all forms of AMA1 examined, consistent with the initial observations from ELISA, immunoblotting, and indirect IFA experiments, with all binding affinities (K_D) in the low nanomolar range (Fig. 3c). The K_D value of WD34 binding to the six variants of *Pf*AMA1 ranged from approximately 1-20 nM with the lowest K_D value observed with 7G8 AMA1 (1.07±0.78 nM) and the highest K_D value observed with HB3 AMA1 (19.7±7.9 nM). In a control experiment, the RON2 peptide bound to AMA1 with a K_D similar to previously reported values[29].

To identify whether WD34 binds directly to or at a site close to the conserved hydrophobic cleft involved in ligand binding, competition ELISAs were performed with two monoclonal antibodies (mAbs 1F9 and 4G2) whose epitopes were proximal to the hydrophobic cleft and are well characterised)[17,24]. Both mAbs inhibited the binding of WD34 in a dose-dependent manner, although, 1F9 appeared to have a greater impact on WD34 binding than 4G2 (Fig. 3d). These data suggest that the WD34 epitope lies between the footprints of mAbs 1F9 and 4G2, which are at opposite ends of the conserved hydrophobic cleft in *Pf*AMA1.

Fig. 2 WD33 and WD34 recognise AMA1 expressed by *P. falciparum*. a. Immunoblotting of saponin lysed late-stage *Pf* 3D7, W2mef, FVO and 7G8 schizonts. Parasite material was electrophoresed on SDS-PAGE gels in reducing or non-reducing conditions. After transfer, membranes were probed with WD34 or WD33 and HRP conjugated anti-myc (9E10) antibody respectively. The monoclonal antibody (mAb) 5G8 that binds a linear epitope near the N-terminus of AMA1 was used as a control (lower panel) **b.** Indirect immunofluorescence of fixed mature 3D7 and W2mef schizonts with pro-domain specific 5G8 mAb, WD33 and WD34 i-bodies.

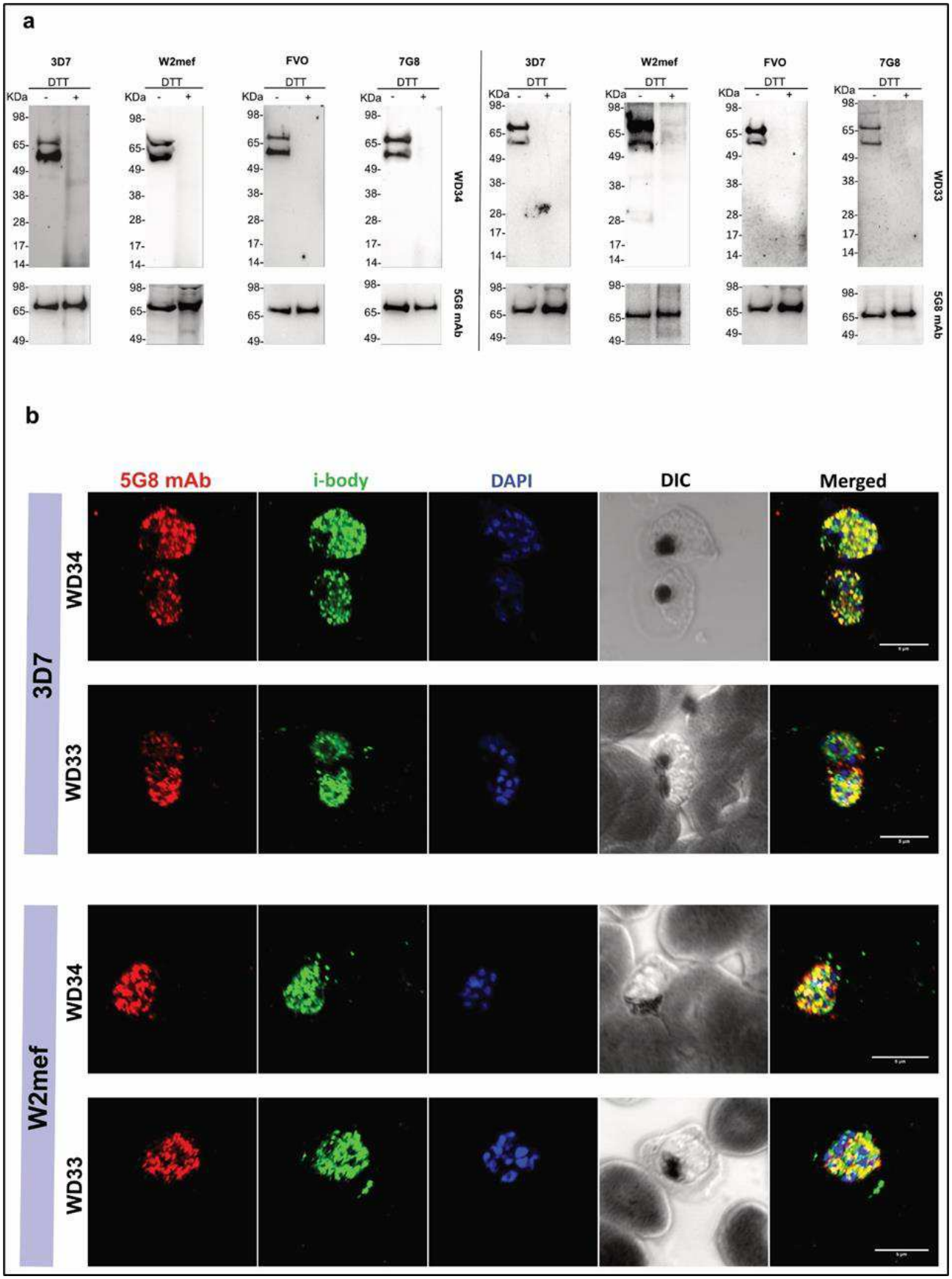
a
3D7
W2mef
FVO
7G8
DTT
KDa
WD34
WD33
5G8 mAb
b
5G8 mAb
i-body
DAPI
DIC
Merged
3D7
W2mef
WD34
WD33

WD34 binds to AMA1 from other *Plasmodium* species

Because their epitope(s) appeared to be highly conserved the WD33 and WD34 i-bodies were tested for binding to recAMA1 from two other *Plasmodium* species; the human parasite *P. vivax* (*Pv* - Palo alto strain) and the murine parasite *P. chabaudi adami* (*Pc* - 556KA strain). WD34 bound to both *Pv* and *Pc*AMA1 indicating that this epitope is conserved not only in *Pf* strains but also in at least some other *Plasmodium* species. WD33 bound to neither *Pv* nor *Pc*AMA1. The affinity of WD34 for *Pv*AMA1 (119±37.3 nM) was approximately 30-fold lower than the average K_D value for *Pf*AMA1 isoforms, and the K_D value for *Pc*AMA1 (26.1 ± 4.08 nM) was approximately 8-fold lower than the average K_D value for *Pf*AMA1 isoforms.

These data indicate that WD34 binds strongly to many isoforms of *Pf*AMA1 and AMA1 from other *Plasmodium* species, despite extensive polymorphic changes in these molecules. The slight differences in K_D values between the different AMA1 variants and WD34 could be due to the involvement of some polymorphic residues in the WD34:AMA1 interaction. The affinity of WD33 for *Pf*AMA1 variants ranged from 10-20 nM, whereas no binding was observed to *Pv* or *Pc*AMA1 (Fig. 3c). These data provide strong evidence that the inhibition of RON2 binding by WD34, but not WD33 was not due to differences in binding affinity of the two i-bodies.

AMA1 interacting residues of WD34 are conserved in *Plasmodium*.

To understand the structural basis of WD34 binding to AMA1 and its pan-specificity we determined crystal structures of WD34 in complex with *Pf* (3D7) recAMA1 and *Pv* (Palo Alto) recAMA1(domain I and II) to resolutions of 2.4 Å and 3 Å, respectively (Fig. 4a-c and Extended Data Table 2). Consistent with previous publications, both *Pf* and *Pv*AMA1 constructs used here adopted the conserved two domain structure previously observed for AMA1[16,17,30-32]. Similarly, WD34 has the typical compact globular structure described for an i-body[25] featuring a series of beta-strands, a canonical disulphide bond in the scaffold, and two loop regions corresponding to CDR1 and CDR3. In both i-body-AMA1 complexes the WD34 footprint spans the conserved hydrophobic cleft in AMA1, perpendicular to the RON2 peptide footprint (Fig. 4d-f). The AMA1 surface area buried by WD34 is 1645 Å and 1972 Å for *Pf* and *Pv*AMA1, respectively. These buried surface areas are remarkably large footprints, particularly considering that WD34 is a single-domain antibody harbouring only two CDRs. Indeed, the observed buried surface areas are larger than the footprints of previously identified invasion inhibitory anti-AMA1 antibodies, including 1F9 (1220 Å in PDB ID: 2Z8V) and IgNAR(14I1-M15) (1205 Å in PDB ID: 2Q8A)[17,32]. In contrast to 1F9 and the IgNAR (14I1-M15), which interact with the highly polymorphic loop 1d of AMA1, WD34 binds mainly to the relatively conserved residues in AMA1 domain I of both *Plasmodium* species, displaying only minor differences in the two binding interfaces (Fig. 4a, b and Extended Fig. 6, 7).

As expected, the CDR1 and CDR3 regions of the i-body are responsible for most of the interactions with AMA1 (Extended Data Table 3). In both complexes, an additional disulphide bond linking CDR1 (C22) and CDR3 (C31) constrains the flexibility of the CDR loops in WD34 (Fig. 4g). This disulphide bond is essential for the interaction of WD34 with AMA1, as mutating C22 and C31 to serine completely abolished the interaction (Fig. 4g). In both complexes, at least 12 out of the 21 CDR residues in WD34 are involved in binding to AMA1

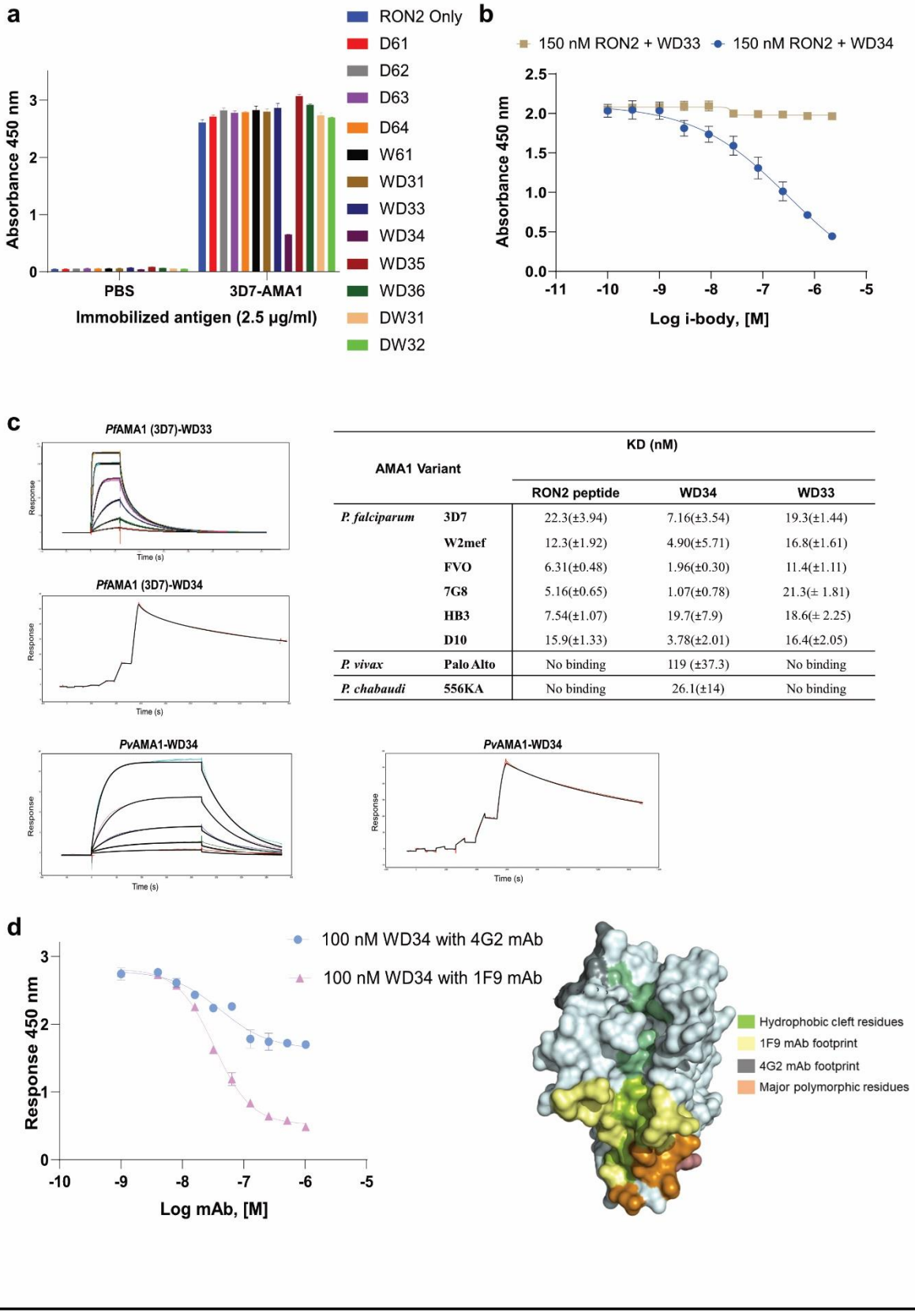

AMA1 Variant		KD (nM)		
		RON2 peptide	WD34	WD33
P. falciparum	3D7	22.3(±3.94)	7.16(±3.54)	19.3(±1.44)
	W2mef	12.3(±1.92)	4.90(±5.71)	16.8(±1.61)
	FVO	6.31(±0.48)	1.96(±0.30)	11.4(±1.11)
	7G8	5.16(±0.65)	1.07(±0.78)	21.3(± 1.81)
	HB3	7.54(±1.07)	19.7(±7.9)	18.6(± 2.25)
	D10	15.9(±1.33)	3.78(±2.01)	16.4(±2.05)
P. vivax	Palo Alto	No binding	119 (±37.3)	No binding
P. chabaudi	556KA	No binding	26.1(±14)	No binding

Fig. 3. Characterisation of the WD33 and WD34 binding interaction with AMA1 a. ELISA showing the binding of the AMA1 specific i-body (150 nM) in the presence of biotinylated RON2 peptide (150 nM) against immobilised AMA1. The remaining AMA1 bound RON2 peptide was measured by using streptavidin HRP. Experiments were performed in triplicate, and error bars represent the standard deviation. **b.** Inhibition of RON2 peptide (150 nM) binding to AMA1 by increasing concentrations of WD34. Experiments were performed in triplicate, and error bars represent the standard deviation. **c.** Determination of equilibrium dissociation constant (K_D) of AMA1 and conformational epitope-specific i-bodies (WD33 & WD34) by Surface Plasmon Resonance. All the generated sensorgrams were analysed by T200 evaluation software. At least three independent experiments were performed to get the final reported values. K_D values were reported at the nanomolar level, and the standard deviation was reported in parenthesis. See extended Data Table 1. **d.** Dose-dependent of inhibition of WD34 binding to AMA1 by 1F9 and 4G2 mAbs that have been previously reported to bind around the hydrophobic cleft (footprints mapped on the structure of AMA1). Experiments were performed in triplicate, and error bars represent the standard deviation.

(Extended Data Table 3). Apart from interacting with the residues in the CDR3 and CDR1 loops of WD34, AMA1 also interacts with WD34 scaffold residues, forming several direct contacts. A detailed description of this interaction is provided in extended data (Extended Fig. 8).

Although the WD34 footprint is nearly identical in size and location in *Pf* and *Pv*AMA1 there are notable differences in the i-body-antigen interactions in the two complexes. WD34 forms more hydrogen bonds with *Pf*AMA1 than with *Pv*AMA1 (Extended Table 3). In the WD34:AMA1^{Pf} complex, G80^{WD34} and W88^{WD34} interact with AMA1 via hydrogen bonds, whereas these residues only create weak van der Waals interactions with *Pv*AMA1. Another point of distinction is the differing mode of engagement with AMA1 Y234. In the WD34:AMA1^{Pf} complex W88^{WD34} contacts Y234^{Pf} via a π stacking interaction (Extended Fig. 9), which is absent in the WD34:AMA1^{Pv} complex. Using FoldX position scan software, we searched for AMA1 interacting residues with the highest free binding energy. Based on calculations of free binding energy changes, the WD34:AMA1^{Pf} complex exhibits more free binding energy than the WD34:AMA1^{Pv} complex, reflecting the higher binding affinity observed in SPR analysis (Extended Fig. 10). This detailed structural information provides a molecular explanation for the observation that WD34 binds to AMA1 from a range of *Plasmodium* species.

Fig. 4. Structural elucidation of AMA1-WD34 interaction a. Crystal structure of WD34: AMA1^{Pf} complex. *Pf* AMA1 is shown in cyan, and WD34 is shown in purple in cartoon representation **b.** Crystal structure of WD34:AMA1^{Pv} complex. *Pv*AMA1 is shown in green, and WD34 is shown in purple in cartoon representation. **c.** Superimposition of WD34:AMA1^{Pf} and WD34: AMA1^{Pv} complexes. **d.** WD34 footprint (purple) on *Pf*AMA1 compared to the hydrophobic cleft (green). The shared footprint is shown in grey. **e.** WD34 footprint (purple) on *Pv*AMA1 compared to the hydrophobic cleft(green). **f.** WD34 footprint (purple) compared to *Pf*RON2 peptide footprint (yellow). The shared region is depicted in orange. **g.** Binding ability of WD34CS mutant. C22^{WD34} and C31^{WD34} residues were mutated to serine residues (and the binding was analysed by ELISA).

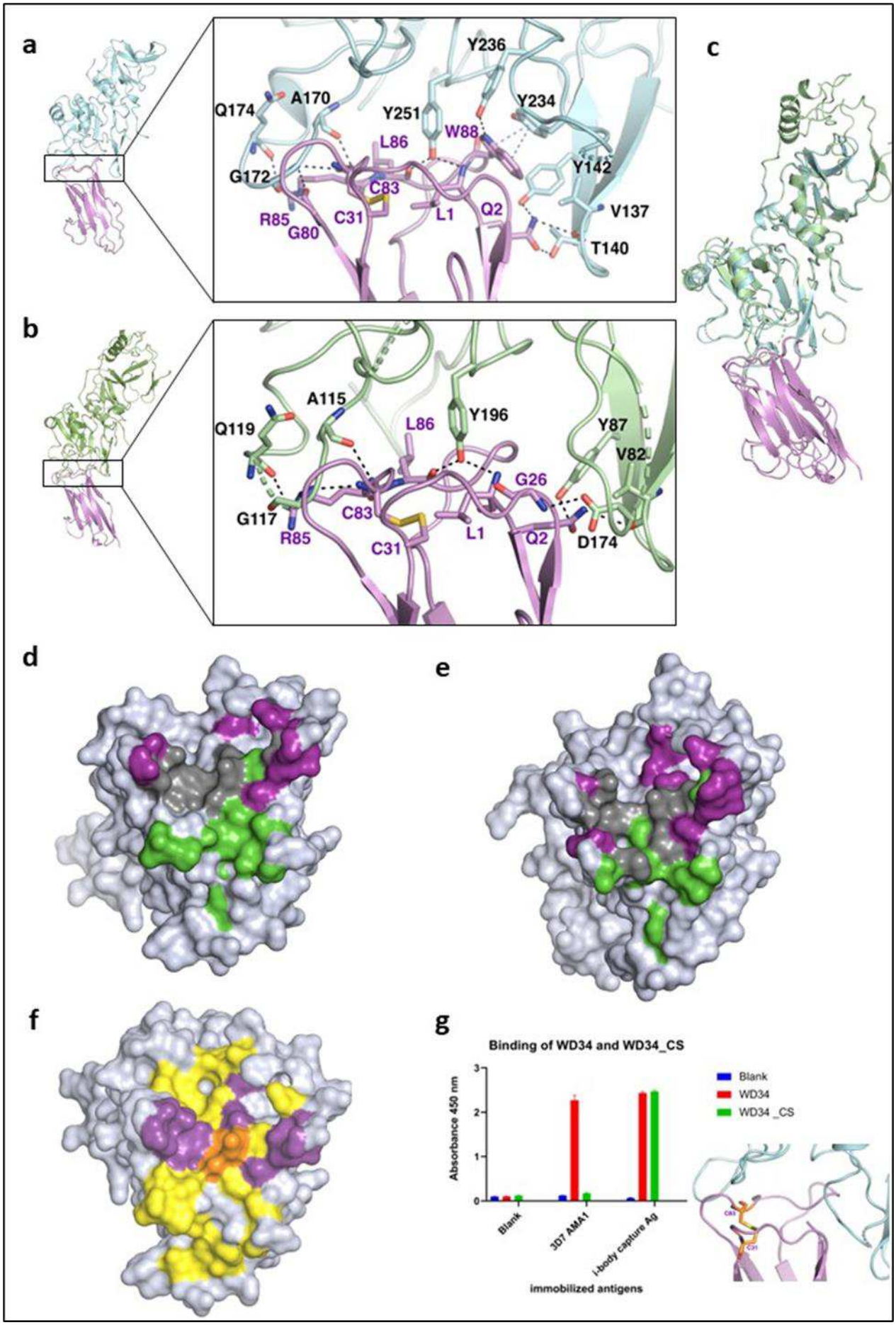
a
Y236
Q174
A170
Y251
Y234
W88
L86
G172
Y142
C83
V137
R85
G80
C31
L1
Q2
T140
b
A115
Q119
L86
Y196
Y87
V82
G26
G117
C83
R85
C31
L1
Q2
D174
c
d
e
f
g
Binding of WD34 and WD34_CS
Absorbance 450 nm
Blank
WD34
WD34 _CS
Blank
3D7 AMA1
i-body capture Ag
immobilized antigens

WD34 inhibits erythrocyte invasion by merozoites of multiple *Plasmodium* species

The inhibitory activity of WD33 and WD34 on parasite growth was tested using a standard parasite growth inhibition assay with wildtype *P. falciparum* 3D7, W2mef, 7G8, Dd2 strains. To determine whether WD34 can inhibit parasites of other species, P. *knowlesi* (a zoonotic parasite) and *Pf*W2mef transgenic parasites expressing AMA1 from *P. vivax* were examined (Fig. 5a, b, c). WD34 inhibited the growth of all parasite lines in a dose-dependent manner with the mean half-maximal inhibitory concentration (IC_{50}) ranging from 13 μg/ml to 128 μg/ml whereas WD33 showed poor inhibitory activity against the *Pf*3D7 parasite line (Fig. 5c). This broadly similar potency of WD34 in inhibiting multiple parasite lines was consistent with the structural and functional data described above. Importantly, the IC_{50} values for WD34 reported here are lower than previously published values for AMA1 antibodies that inhibit merozoite invasion[33,34].

WD34 inhibits sporozoite invasion of hepatocytes,

Previous reports have established that the AMA1:RON2 complex is involved in sporozoite hepatocyte invasion, and an inhibitory R1 peptide also impaired cell traversal by *P. falciparum* sporozoites suggesting AMA1 may be involved in establishing *Plasmodium* liver-stage infection[11,12,35]. To investigate the effect of WD34 on cell traversal, salivary gland sporozoites of the *Pf*NF54 strain were incubated with HC-04 hepatocytes in the presence of fluorescein isothiocyanate (FITC)-dextran and increasing concentrations of WD34. The dose-dependent presence of WD34 did not significantly inhibit hepatocyte traversal when compared to the negative control i-body; 21H5 (Fig. 5d). This finding with *P. falciparum* sporozoites aligned with the recent observations made by Fernandes, et al. [12] that conditional loss of AMA1 and RON2 did not affect *P. berghei* sporozoite migration.

To test the effect of WD34 on hepatocyte invasion by NF54, sporozoites were incubated with HC-04 cells in the presence of the i-body, and the number of cells containing intracellular parasites were quantified using flow cytometry 24 h after the treatment with increasing concentrations of WD34. Hepatocyte invasion was significantly inhibited by WD34 in a dose dependent manner confirming that this i-body could prevent sporozoite invasion. There results were also consistent with AMA1:RON2 interaction being important for *P. falciparum* sporozoites invasion of hepatocytes[11,12,35] (Fig. 5e).

Fig. 5. Inhibition profile of WD34 in merozoite growth and sporozoite activity. **a**. Inhibition of merozoite growth by WD34 in multiple parasite lines was tested. Growth inhibition assays were performed as a two-fold dilution series of WD34. Data represents the mean of three independent experiments. Error bars represent the standard deviation. **b.** Growth inhibition of *Pf*3D7 parasite line by WD33. Growth inhibition assays were performed as a two-fold dilution series of WD33 starting at 1 mg/ml. Three independent experiments with three replicates were performed, and data points represent the mean values. Error bars represent the standard deviation**. c.** IC_{50} values for each parasite line. The non-linear regression model interpolated values generated from the inhibition data**. d-e.** i-body inhibition effect against *P. falciparum* hepatocyte traversal (**d**) and invasion (**e**). Number of FITC-Dextran+ HC-04 cells or HC04 cells with intracellular sporozoites treated with WD34 or 21H5 at three and 24 hrs post sporozoite infection normalised to *Pf*NF54 control. The FITC-Dextran background was subtracted from each sample for the three-hour timepoint. The mean of biological triplicates and the standard deviation is shown. Statistical analysis: Friedman test (non-parametric) with multiple comparisons against *Pf*NF54. **$p < 0.01$; *$p < 0.05$.

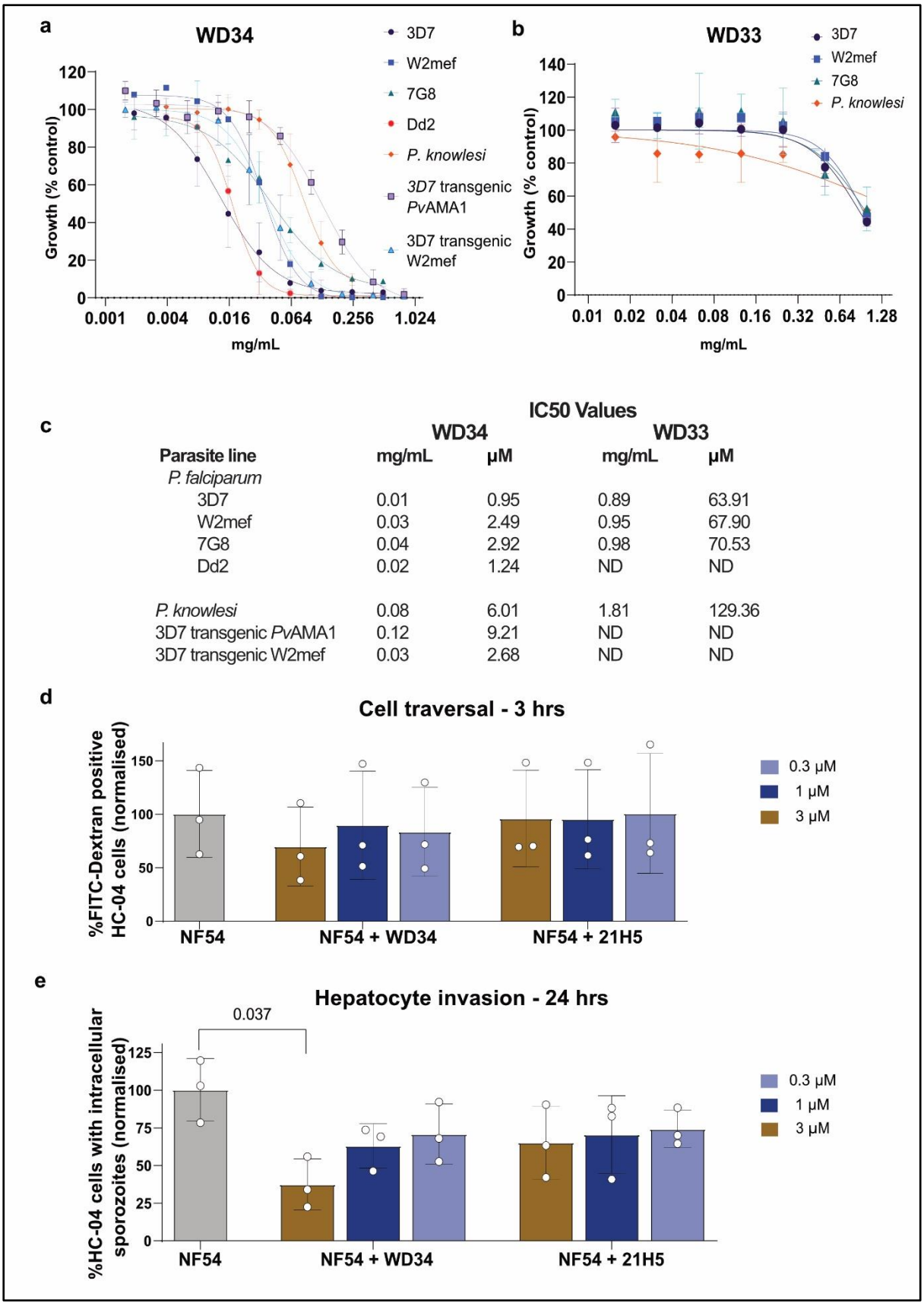

c

IC50 Values

Parasite line	WD34 mg/mL	WD34 µM	WD33 mg/mL	WD33 µM
P. falciparum				
3D7	0.01	0.95	0.89	63.91
W2mef	0.03	2.49	0.95	67.90
7G8	0.04	2.92	0.98	70.53
Dd2	0.02	1.24	ND	ND
P. knowlesi	0.08	6.01	1.81	129.36
3D7 transgenic *Pv*AMA1	0.12	9.21	ND	ND
3D7 transgenic W2mef	0.03	2.68	ND	ND

Discussion

AMA1 has been studied extensively as a potential component of a vaccine against *P. falciparum* malaria. However, like most *P. falciparum* merozoite proteins that are natural immunogens, AMA1 is highly polymorphic, and this has prevented the generation of broadly protective immune responses in field trials with AMA1-containing vaccines[19,36-38]. Here we have used an i-body (WD34) isolated from a phage-display library to identify a previously unrecognised highly conserved epitope in AMA1. To isolate WD34 and other cross-reactive i-bodies we used a cross-panning strategy on *Pf*3D7 and *Pf*W2mef recAMA1, which were chosen because of their extensive sequence differences[28]. In contrast to the cross-reactive characteristics of the i-bodies selected using the cross-panning strategy i-bodies selected by direct panning on one or other of the recAMA1 isotypes were more strain-specific.

WD34 reacted strongly with both isoforms of AMA1 used in the cross-panning strategy to select this i-body and with the four other isoforms of *Pf*AMA1 examined. To our surprise, WD34 also cross-reacted with AMA1 of *P. vivax* (Palo Alto strain), the other major cause of human malaria, with AMA1 of *P. knowlesi*, which causes malaria in humans and other primates, and AMA1 of the rodent parasite, *P. chabaudi adami* (556KA strain).

Using rec*Pf*AMA1 and a *Pf*RON2 synthetic peptide we showed that WD34 blocked the interaction between AMA1 and its RON2 ligand, which is inserted by the parasite into the erythrocyte cell membrane prior to merozoite invasion. As WD34 also blocked the binding of mAbs 1F9 and 4G2, whose epitopes lie at opposite ends of the RON2-binding cleft, we concluded that the WD34 epitope lies in the central region of this hydrophobic cleft. This was confirmed by solving the X-ray crystal structures of the WD34:AMA1^{Pf} and WD34:AMA1^{Pv} complexes to resolutions of 2.4 Å and 3 Å, respectively. The WD34 footprint included relatively conserved residues in the central region of the RON2 binding cleft of both the *Pf* and *Pv* isoforms of AMA1, distant from the highly polymorphic loop 1d in *P. falciparum*, which is targeted by the "strain-specific" mAb, 1F9[17].

In both complexes, WD34 contacts a small number of residues in the hydrophobic cleft thatare directly involved in RON2 binding, but most of the WD34 contacts are with surrounding residues on both sides of the cleft in loops 1a, 1b, 1c and 1e (Extended Fig. 11.). Notably, five out of the six WD34 contact residues are strictly conserved in AMA1 of *Plasmodium* isolates collected in multiple countries where malaria is endemic and only one residue (G172) is clearly polymorphic. In ~32% of the *Pf*AMA1 sequences surveyed and in the HB3 isoform studied here, G172, which makes contacts with WD34 G80 in the crystal structure, is mutated to glutamic acid (Extended Fig. 12). This difference may be responsible for the WD34 binding affinity for HB3 *Pf*AMA1 (K_D = 19.7 nM) being slightly lower than for the other five *Pf*AMA1 isoforms studied (K_D = 1.07–7.16 nM). In < 1% of parasites surveyed this residue was mutated to either valine or arginine but the effect of this mutation on WD34 binding affinity has not been examined (Extended Fig. 13).

The finding that the binding affinity of WD34 for *Pv*AMA1 was approximately 30-fold less than its binding affinity for *Pf*AMA1 is not surprising given that WD34 was selected by panning the i-body-phage library on *Pf*3D7 AMA1. Although there are many conserved features to the WD34 epitope in the two forms of AMA1, there are also differences in the two interfaces, which could account for the difference in binding affinity. Notably, WD34 forms more polar interactions with *Pf*AMA1 than with *Pv*AMA1 (Extended data, Table 3). For

example, G80and W88 of WD34 form hydrogen bonds to *Pf*AMA1 G172 (3.2 Å) and 2.82 Å Y236 (2.82 Å), respectively, but equivalent interactions are lacking in the WD34:AMA1^{Pv} complex.

A characteristic property of camelid (nanobodies) or shark single-domain antibodies (VNARs) is their ability to interact via their extended CDR3 loop with concave epitopes not accessible to conventional antibodies[39]. The WD34 i-body studied here also has an extended CDR3 loop, but rather than penetrating the hydrophobic RON2 binding cleft of AMA1 like the IgNAR (14I1-M15), the CDR3 and CDR1 loops, with some framework residues, form a paratope that spans the RON2-binding cleft when WD34 binds to AMA1[32]. Despite the small size of the i-body compared to conventional antibodies the WD34 footprint is considerably larger than previously characterised anti-AMA1 antibodies[17,32]. This may, at least partly, be due to the disulphide bond between CDR1 and CDR3 facilitating a spatial arrangement of the CDR loops that provides a flattened paratope surface. An important consequence of the large interface between WD34 and the surface of AMA1 may be a tolerance of polymorphisms, contributing to the broad cross-reactivity described here.

Although there is evidence suggesting some forms of AMA1 bind to other ligands, binding of *Pf*AMA1 to *Pf*RON2 is essential for the invasion of host cells by merozoites and sporozoites[8-13,40,41]. As expected for a reagent that blocks access to the RON2 binding cleft on AMA1, WD34 inhibited the invasion of erythrocytes and hepatocytes by *P. falciparum* merozoites and sporozoites, respectively. The inhibitory potency of WD34 in merozoite growth inhibitory assays was broadly similar for multiple strains of *P. falciparum* and for *P. knowlesi* with the IC_{50} values reported here being some of the lowest for an "antibody" recognizing multiple parasite lines. To our knowledge, this is the first time a pan-species-specific anti-AMA1 reagent with potent invasion inhibitory properties has been reported. Previously, Collins, et al. [24] and Igonet, et al. [23] described two AMA1 monoclonal antibodies with broad strain and species specificity, however, both those antibodies showed rather poor *in-vitro* invasion inhibitory activity[23,34,42].

Malaria vaccine development has made important advances in the last decade with two vaccines targeting *P. falciparum* sporozoites now approved for use[43-46]. As discussed earlier, the polymorphisms in AMA1 have proven to be a major barrier to efforts aimed at developing a vaccine incorporating this asexual blood-stage antigen. One approach to overcoming this problem has been to immunise with an AMA1:RON2 complex. This approach has shown promise in preclinical studies and has demonstrated that there are conserved epitopes in AMA1 that can be targeted by protective antibodies[47-49]. However, it is not yet clear whether the highly conserved WD34 epitope can be targeted by a natural antibody response or antibodies induced by vaccination. If a form of AMA1 can be engineered that diverts the induced antibody response away from highly polymorphic regions, such as loop 1d, towards relatively conserved regions such as the WD34 footprint defined here, the potential of AMA1 as a vaccine candidate may be re-examined. However, this may be challenging particularly if the recently described process of antigenic diversion, in which non-neutralising mAbs to overlapping epitopes outcompete a parasite-neutralising mAb binding to a conserved *Pf*MSP1 epitope, also applies to AMA1[50]. It is also possible that the WD34 epitope is poorly immunogenic, and its identification here may have resulted from the use of the large naive i-body library in which the range of CDR sequences was not restricted by immunisation or infection, which usually proceeds the creation of nanobody or monoclonal antibody libraries.

In recent years evidence has accumulated showing that the control of malaria with drugs and a vaccine may be complemented by immunotherapy with human monoclonal antibodies[51-53]. The human mAb, CIS43LS, which targets *Pf*CSP, protected human volunteers against challenge with *P. falciparum* when administered subcutaneously at low doses[54]. Although the major focus of current immunotherapy studies has been the sporozoite antigen CSP, if one aim is to reduce morbidity and mortality, immunotherapy with antibodies targeting asexual blood-stage antigens should be considered as a complement to chemotherapy[55]. AMA1 is an attractive candidate for this approach as it is expressed in both asexual and sexual stages of the parasite life cycle. The WD34 i-body in its current small, single-domain form is not a candidate for assessment as an immunotherapeutic, however, we have generated an Fc-tagged version of WD34 that binds with high affinity to AMA1 from different strains and species of *Plasmodium*. Moreover, WD34 in this format can also inhibit merozoite and sporozoite invasion (published in future publications). It should be noted that AD-214, an i-body with a human Fc, has been shown to be safe and well tolerated in a human Phase 1 safety and tolerability study in healthy volunteers (ClincalTrials.gov: NCT04415671) suggesting a potential future pathway for a WD34 derived antibody-based therapeutic against malaria.

Methods

Mammalian cells, parasite cultures, peptides, and antibodies

Expi293 and ExpiCHO (ThermoFisher) cells were maintained in Expi293 and ExpiCHO expression mediums (ThermoFisher) at 37 °C, 8% CO_2, 125 r.p.m. 3D7, DD2, 7G8, FVO and W2mef *P.falciparum* and *P. knowlesi* parasites were maintained in *in-vitro* cultures at 37 °C according to previously published protocols[56,57]. Biotin-tagged and untagged RON2 peptide (DITQQAKDIGAGPVASCFTTRMSPPQQICLNSVVNTALSTSTQSAMK) with cyclised cysteines were synthesised by Mimotopes, Australia.

In this study, 4G2 rat mAb, 1F9 mAb and 5G8 mAb were obtained from Robin Anders. Anti-c-myc mAb (9E10), and anti-i-body scaffold mAb (7G4) were made at the WEHI Antibody Facility, Bundoora, Australia. Fluorophore and HRP conjugated antibodies were used as follows: Anti-M13 HRP (catalogue no: 11973-MM05T-H, Sino Biological), anti-his HRP mAb (catalogue no: A7058, Sigma-Aldrich), goat anti-human IgG (Fc specific) HRP (catalogue no: A0170, Sigma-Aldrich), goat anti-mouse IgG (catalogue no: AP127P, Sigma-Aldrich), Streptavidin HRP (catalogue no: 21130, ThermoFisher), goat anti-human Alexa fluor 488 (catalogue no: H10120, Invitrogen), goat anti-rabbit Alexa Fluor 568 (catalogue no: A11036, Molecular Probes), goat anti-rabbit 546 (catalogue no: A11081, Invitrogen), goat anti-mouse 568 (catalogue no: A11031, Invitrogen), goat anti-mouse FITC (catalogue no: F0257, Sigma Aldrich).

Expression and purification of *Pf*AMA1 isoforms, *Pv*AMA1 and *Pc*AMA1

Codon-optimised full ectodomain (domain I, II and II) of *Pf*3D7, W2mef, 7G8, FVO, HB3, D10 and *Pc*AMA1 sequences were cloned into pET-28a (+)-Tev vector (Genscript, Singapore). AMA1 protein was expressed in inclusion bodies, purified and refolded according to the standard protocols[16,58]. The codon optimised *Pv*AMA1 (Palo Alto) sequence in PcDNA3.1 was kindly provided by James Beeson, Burnet Institute. *Pv*AMA1 was expressed in Expi293 cells and purified from the Expi293 expression medium using Ni-NTA chromatography.

Biopanning using phage-displayed i-body library

Phage affinity panning was performed as described previously with some modifications[25,32]. i-body phage-displayed library (~10^{10} random i-body sequences cloned into pADL-23c phagemid vector) was amplified in *E. coli* TG1 cells. At OD_{600}= 0.4–0.5, *E. coli* TG1 cells infected with M13K07 helper phage (Antibody design laboratories, USA) to allow the i-body to be displayed on phage particles. The amplified i-body phage library was biopanned independently on immobilised recombinant *Pf*3D7 and *Pf*W2mef AMA1 (2.5 µg/ml). Six rounds were carried out with each biopanning campaign. For cross-biopanning, a portion of the round three phage at each panning campaign was incubated with immobilised recombinant AMA1 of the other isoform (from *Pf*3D7 enriched phage to *Pf*W2mef AMA1 and vice versa). These then underwent a further three rounds of biopanning.

Phage enrichment ELISA, single clone screening and sequencing

Phage ELISAs were performed as described previously[25]. Briefly, 96 well plates (Nunc, Maxisorp) were coated with the antigens and blocked with 5% skim milk. Amplified phage pools eluted from the rounds or single clone phage were incubated in 1:10 dilution against immobilised antigens. The wells were washed three times with 0.1% PBST, and bound phage were detected with horseradish peroxidase tagged anti-M13 antibody (Sino-biologicals) followed by 3,3',5,5'-tetramethylbenzidine (ThermoFisher) as enzyme substrate. Enzyme reaction was stopped with 0.1 M HCl, and absorbance was measured at 450 nm.

Phage-infected TG1 single colonies were grown as 2 ml cultures in 48 deep well plates (Corning Axygen) and induced with 1 mM IPTG for i-body expression for 16 hours. The level of i-body expression and AMA1 binding from periplasmic extracts of each clone were assessed by ELISA. The positive clones for both i-body expression and AMA1 binding were sequenced by Sanger sequencing at the Australian Genome Research Facility, Melbourne, Australia.

Expression and purification of i-bodies

AMA1-specific i-body sequences in pADL-23c vector plasmids (Antibody Design Laboratories, USA) were transformed into *E. coli* BL21 cells. Bacteria grown overnight in 2YT media supplemented with 0.1% (w/v) glucose and ampicillin (100 µg/ml) at 37 °C were diluted to OD_{600} of 0.1 and incubated at 37°C. At OD_{600} = 0.7, BL21 cells were induced with 1 mM IPTG and subjected to a further growth overnight at 28°C. Periplasmic extraction of the i-bodies was conducted as described previously[59]. Briefly, the centrifuged cell pellet was

resuspended in the full-strength spheroplast buffer with lysozyme and incubated in ice for ten minutes, followed by incubation in half-strength spheroplast buffer. The periplasmic fraction was isolated by centrifugation, and i-bodies were purified by immobilised metal affinity chromatography (IMAC) followed by ion-exchange chromatography (Cytiva-CaptoQ) size exclusion chromatography.

Sequences of human and mouse IgG1 Fc region-tagged i-bodies were designed by cloning into a PcDNA3.1 vector (Genscript, Singapore) to express i-body Fc versions in Expi293 and ExpiCHO (Invitrogen, USA) expression systems. Fc-tagged i-bodies were purified using affinity purification (Mabselect PrismA- Cytiva) and size exclusion chromatography.

Standard and competition ELISA

Indirect i-body binding ELISAs were used to determine the specificity of AMA-1-specific i-bodies. All incubations were performed at 100 µl per well at room temperature for 1 hour or overnight at 4^{o}C. Washing steps included at least three washes with 0.1% PBST. RON2 peptide blocking screening was performed by incubating the same concentrations (50 nM) of biotin-tagged RON2 peptide and i-body mixture against immobilised *Pf*3D7 AMA1 at 2.5 µg/ml) and measuring the bound RON2 peptide by using streptavidin HRP.

Competition ELISA of RON2 peptide and i-bodies was performed as 150 nM biotin-tagged RON2 peptide and increasing concentrations of WD34 and WD33 i-bodies were incubated against immobilised *Pf*3D7 AMA1 at 2.5 µg/ml. Bound RON2 peptide was measured using streptavidin HRP.

Competition ELISA of WD34 with 1F9 and 4G2 mAbs anti-AMA1 mAbs was performed with100 nM of human Fc-tagged WD34 and increasing concentration of both 1F9 and 4G2 mAbs. This mixture was added to immobilised *Pf*3D7 AMA1 and bound WD34 measured using goat anti-human Fc specific HRP antibody.

Immunoblotting and immunofluorescence of recombinant proteins and schizonts

Saponin lysed late-stage schizonts were pelleted, further lysed with lamellae buffer, and subjected to SDS gel electrophoresis on 4 - 12% acrylamide gels (BOLT, Invitrogen). Proteins were transferred to nitrocellulose membrane for 7 minutes (iBlot2, Invitrogen), blocked with 10% skim milk and probed with 10 µg/ml of i-bodies (in 5% skim milk). Membranes were then washed three times with 0.05% PBST and incubated with anti-Fc secondary antibodies. Western blots were developed with West Pico PLUS chemiluminescent reagents (ThermoFisher, USA) and visualised using the Biorad GelDoc system.

For fixed immunofluorescence imaging, smears of synchronised late-stage schizonts on glass microscope slides were fixed with 100% methanol for 2 minutes and incubated in a blocking buffer (4% BSA in PBS) for at least 1 hour. Fc-tagged i-bodies (10 µg/ml), and fluorophore-

tagged secondary antibodies (1:1000) were used. Labelled parasites were imaged with a Zeiss LSM 880 inverted microscope with x63/1.4 oil objective, appropriate excitations, and an Airyscan detector. Captured images were analysed with ImageJ software.

Surface Plasmon Resonance studies

Kinetic analysis and equilibrium dissociation constants (K_D) were measured using Biacore T200 (Cytiva). The surfaces of flow cells one, two and four were activated for 14 minutes with a 1:1 mixture of 0.1 M NHS and 0.4 M EDC at a 5 µl/min flow rate. The ligands (AMA1) at a concentration of 80 µg/ml in 10 mM sodium acetate, pH 4.5, were immobilised at a density of 500 RU on the flow cells two and four. Flow cell one was immobilised with bovine serum albumin to serve as a reference surface. All the surfaces were blocked with a 7-minute injection of 1 M ethanolamine, pH 8.0. i-bodies (14 kDa, 90% purity based on SDS–PAGE) in 10 mM Tris, 150 mM NaCl,0.005% Tween-20,1% BSA pH 8, were injected over the flow cells at a concentration range from 50 µM to 0.156 nM at a flow rate of 45 µl/min and at a temperature of 25°C. Both multi-cycle kinetic and single-cycle kinetic analyses were used to describe the AMA1-i-body interactions.

Structure determination of the AMA1-WD34 complexes

WD34-bound *Pf*AMA1 and *Pv*AMA1 protein samples were prepared for crystallisation as described previously [25]. The protein:protein complexes were in 50 mM Tris, and the initial sparse matrix crystallisation trials were performed in 96-well sitting drop trays (Swissci, Neuheim, Switzerland) at a molar ratio of 1:1 using an in-house Gryphon LCP (Art Robbins Instruments). Initial protein samples were set up at 0.2 µl of protein sample and 0.2 µl reservoir per drop. Subsequent crystal optimisation trials were conducted in 24-well Limbro plates (Hampton Research). All crystallisation trials were performed at 20°C. *Pf*AMA1-WD34 complex crystals were obtained in 0.1M HEPES, 70% MPD, pH 7.5 at 5 mg/ml concentration and *Pv*AMA1-WD34 complex was obtained in 0.1 M MES,12% w/v PEG20000, pH 6.5 at 5 mg/ml concentration.

X-ray diffraction data was collected at the MXII beamline of Australian synchrotron. Data were processed to 2.7Å for WD34:AMA1^{Pf} and 3Å for WD34:AMA1^{Pv} using XDS package (Kabsch, 2010). Structures were solved by molecular replacement in Phaser using the structural coordinates of PDB IDs - 1Z40 (*Pf*AMA1), 5NQF (*Pv*AMA1) and 5AEA (i-body scaffold). Structure building and refinement were performed in Coot. The atomic coordinates and structure files were deposited in the Protein Data Bank under PDB ID 8QU7 (WD34:AMA1^{Pf}) and 8QUS (WD34:AMA1^{Pv}). All the figures of the structures were prepared by using PyMOL[60].

Blood-stage invasion inhibition assays

Two-cycle growth inhibition assays were performed as follows: synchronised ring-stage parasites were diluted to 0.5% parasitemia and 1% (v/v) haematocrit in 25 µL RPMI 1640, 25 mM HEPES media with i-bodies and added into 96-well round-bottomed culture plate. Parasites were incubated for 48 hours at 37°C. After 48 hours parasites were washed with PBS and stained with 10 µg/mL ethidium bromide (BioRad) and 1 x 10^5 erythrocytes were counted by using an Accuri flow cytometer (BD Biosciences).

Invasion inhibition assays for transgenic parasites

Invasion assays were performed as previously described, with minor changes[61]. Parasites were synchronised with sorbitol, then inoculated at late trophozoite and schizont stages at 0.5% parasitaemia in 4% haematocrit in 45 µl RPMI media, with 5 µl i-bodies in PBS. Cultures were left to invade, then harvested at ring stage by fixation with 0.25% glutaraldehyde. Parasites were stored in PBS at 4°C. Cultures were later stained with 1× SYBR Green I (S7563, Invitrogen), and parasitaemia assayed by flow cytometry in a BD FACSCanto™ II system, with further analysis in FlowJo™ v10.9.0 (BD Life Sciences). Parasites were gated from uninfected erythrocytes using the FITC-A and PE-A channels. Net growth rates were calculated by subtracting the parasitaemia of parasites inoculated with 1 mg/ml heparin, then dividing by the parasitaemia of parasites inoculated with 5 µl PBS. Growth percentages were subtracted from 100% to give invasion inhibition.

IC50 calculations were performed in R using the packages drc and ggplot2 [61-64]. Assays were performed in biological triplicate, and IC50s calculated independently for each replicate. The parasite lines used were based on W2mef, with the AMA1 locus replaced with either the P. vivax locus or the P. falciparum 3D7 version[28,65].

Sporozoite cell traversal and hepatocyte invasion assays

HC04 hepatocytes were seeded at confluence (100,000 cells per well) in a 96-well plate. Sporozoites were extracted and resuspended in IMDM + 5% FBS + 0.5 mg/mL dextran-FITC at a final concentration of 450 sporozoites/µL (Multiplicity of infection (MOI): 0.45). i-bodies were added and incubated with sporozoites and dextran for 15 minutes on ice. Monoclonal antibody 2A10 against *P. falciparum* CSP was used as a positive control at 10 µg/ml concentration. After incubation, sporozoites were added to cells and spun down at 500 x g for 3 minutes. After 4h of incubation, cells were trypsinised, and half of the cells were processed for traversal read out (Dextran FITC) and the other half were replated for an invasion read out at 24 hours post infection (CSP conjugated to ALEXA 647)

Data availability

The crystal structures reported in this manuscript are deposited in the Protein Data Bank, www.rcsb.org (PDB IDs 8QU7 and 8QUS).

Acknowledgements

We thank Dr Kaye Truscott and Deepti Verghese-Jose for facilitating the protein purification in MBB laboratory (La Trobe University), A/Professor Hamsa Puthalakath for plasmids, Dr Chris Szeto and Professor Stephanie Gras for training on SPR, Liana Theoridis and Dr Teresa Carvalho for supplying parasites for initial experiments, Ornella Romeo at Adelaide University for preparation of parasite samples, La Trobe Proteomics and Metabolomics Platform and Bioimaging Facility for facilitating SPR and confocal imaging, AdAlta for providing reagents and consumables to conduct the study, Australian Red Cross Blood Service for blood. X-ray crystallographic data were acquired by using the MX2 beamline at Australian Synchrotron, The Australian Nuclear Science and Technology Organization. Dimuthu Angage was offered La Trobe University Graduate Research Scholarship (LTGRS), and La Trobe University Full Fee Research Scholarship (LTUFFRS) to conduct this study. J.A.B acknowledges NHMRC Investigator Grant 1176955.

Competing Interests

The authors have declared that no conflict of interest exists. This study was a collaboration between AdAlta Limited and La Trobe University. M.F. is Founding Chief Scientist and a shareholder in AdAlta Ltd. R.F.A is a shareholder in AdAlta.

References

1 Miller, L. H., Ackerman, H. C., Su, X.-z. & Wellems, T. E. Malaria biology and disease pathogenesis: insights for new treatments. *Nature Medicine* **19**, 156-167 (2013). https://doi.org:10.1038/nm.3073

2 Gaur, D., Mayer, D. C. G. & Miller, L. H. Parasite ligand–host receptor interactions during invasion of erythrocytes by Plasmodium merozoites. *International Journal for Parasitology* **34**, 1413-1429 (2004). https://doi.org:https://doi.org/10.1016/j.ijpara.2004.10.010

3 Baum, J., Maier, A. G., Good, R. T., Simpson, K. M. & Cowman, A. F. Invasion by P. falciparum Merozoites Suggests a Hierarchy of Molecular Interactions. *PLOS Pathogens* **1**, e37 (2005). https://doi.org:10.1371/journal.ppat.0010037

4 Aikawa, M., Miller, L., Johnson, J. & Rabbege, J. Erythrocyte entry by malarial parasites. A moving junction between erythrocyte and parasite. *Journal of Cell Biology* **77**, 72-82 (1978). https://doi.org:10.1083/jcb.77.1.72

5 Barry, A. E. & Arnott, A. Strategies for Designing and Monitoring Malaria Vaccines Targeting Diverse Antigens. *Frontiers in Immunology* **5** (2014). https://doi.org:10.3389/fimmu.2014.00359

6 Mitran, C. J. & Yanow, S. K. The Case for Exploiting Cross-Species Epitopes in Malaria Vaccine Design. *Frontiers in Immunology* **11** (2020). https://doi.org:10.3389/fimmu.2020.00335

7 Burns, A. L. *et al.* Targeting malaria parasite invasion of red blood cells as an antimalarial strategy. *FEMS Microbiology Reviews* **43**, 223-238 (2019). https://doi.org:10.1093/femsre/fuz005

8 Besteiro, S., Michelin, A., Poncet, J., Dubremetz, J.-F. & Lebrun, M. Export of a Toxoplasma gondii Rhoptry Neck Protein Complex at the Host Cell Membrane to Form the Moving Junction during Invasion. *PLOS Pathogens* **5**, e1000309 (2009). https://doi.org:10.1371/journal.ppat.1000309

9 Riglar, D. T. *et al.* Super-Resolution Dissection of Coordinated Events during Malaria Parasite Invasion of the Human Erythrocyte. *Cell Host & Microbe* **9**, 9-20 (2011). https://doi.org:https://doi.org/10.1016/j.chom.2010.12.003

10 Srinivasan, P. *et al.* Binding of Plasmodium merozoite proteins RON2 and AMA1 triggers commitment to invasion. *Proceedings of the National Academy of Sciences* **108**, 13275-13280 (2011). https://doi.org:doi:10.1073/pnas.1110303108

11 Yang, A. S. P. *et al.* AMA1 and MAEBL are important for Plasmodium falciparum sporozoite infection of the liver. *Cellular Microbiology* **19**, e12745 (2017). https://doi.org:https://doi.org/10.1111/cmi.12745

12 Fernandes, P. *et al.* The AMA1-RON complex drives Plasmodium sporozoite invasion in the mosquito and mammalian hosts. *PLOS Pathogens* **18**, e1010643 (2022). https://doi.org:10.1371/journal.ppat.1010643

13 Loubens, M. *et al.* Plasmodium sporozoites on the move: Switching from cell traversal to productive invasion of hepatocytes. *Molecular Microbiology* **115**, 870-881 (2021). https://doi.org:https://doi.org/10.1111/mmi.14645

14 Drew, D. R. *et al.* Functional Conservation of the AMA1 Host-Cell Invasion Ligand Between P. falciparum and P. vivax: A Novel Platform to Accelerate Vaccine and Drug Development. *The Journal of Infectious Diseases* **217**, 498-507 (2017). https://doi.org:10.1093/infdis/jix583

15 Kennedy, M. C. *et al.* In vitro studies with recombinant Plasmodium falciparum apical membrane antigen 1 (AMA1): production and activity of an AMA1 vaccine and generation of a multiallelic response. *Infect Immun* **70**, 6948-6960 (2002). https://doi.org:10.1128/IAI.70.12.6948-6960.2002

16 Bai, T. *et al.* Structure of AMA1 from Plasmodium falciparum reveals a clustering of polymorphisms that surround a conserved hydrophobic pocket. *Proceedings of the National Academy of Sciences* **102**, 12736-12741 (2005). https://doi.org:doi:10.1073/pnas.0501808102

17 Coley, A. M. *et al.* Structure of the malaria antigen AMA1 in complex with a growth-inhibitory antibody. *PLoS pathogens* **3**, 1308-1319 (2007). https://doi.org:10.1371/journal.ppat.0030138

18 Hodder, A. N., Crewther, P. E. & Anders, R. F. Specificity of the protective antibody response to apical membrane antigen 1. *Infect Immun* **69**, 3286-3294 (2001). https://doi.org:10.1128/iai.69.5.3286-3294.2001

19 Thera, M. A. *et al.* A Field Trial to Assess a Blood-Stage Malaria Vaccine. *New England Journal of Medicine* **365**, 1004-1013 (2011). https://doi.org:10.1056/NEJMoa1008115

20 Remarque, E. J., Faber, B. W., Kocken, C. H. M. & Thomas, A. W. A diversity-covering approach to immunization with Plasmodium falciparum apical membrane antigen 1 induces broader allelic recognition and growth inhibition responses in rabbits. *Infect Immun* **76**, 2660-2670 (2008). https://doi.org:10.1128/IAI.00170-08

21 Dutta, S. *et al.* Overcoming antigenic diversity by enhancing the immunogenicity of conserved epitopes on the malaria vaccine candidate apical membrane antigen-1. *PLoS pathogens* **9**, e1003840-e1003840 (2013). https://doi.org:10.1371/journal.ppat.1003840

22 Kusi, K. A. *et al.* Safety and immunogenicity of multi-antigen AMA1-based vaccines formulated with CoVaccine HT™ and Montanide ISA 51 in rhesus macaques. *Malaria Journal* **10**, 182 (2011). https://doi.org:10.1186/1475-2875-10-182

23 Igonet, S. *et al.* Cross-reactivity Studies of an Anti-Plasmodium vivax Apical Membrane Antigen 1 Monoclonal Antibody: Binding and Structural Characterisation. *Journal of Molecular Biology* **366**, 1523-1537 (2007). https://doi.org:https://doi.org/10.1016/j.jmb.2006.12.028

24 Collins, C. R., Withers-Martinez, C., Hackett, F. & Blackman, M. J. An Inhibitory Antibody Blocks Interactions between Components of the Malarial Invasion Machinery. *PLOS Pathogens* **5**, e1000273 (2009). https://doi.org:10.1371/journal.ppat.1000273

25 Griffiths, K. *et al.* i-bodies, Human Single Domain Antibodies That Antagonize Chemokine Receptor CXCR4*. *Journal of Biological Chemistry* **291**, 12641-12657 (2016). https://doi.org:https://doi.org/10.1074/jbc.M116.721050

26 Cao, Q. *et al.* A single-domain i-body, AD-114, attenuates renal fibrosis through blockade of CXCR4. *JCI Insight* **7** (2022). https://doi.org:10.1172/jci.insight.143018

27 Qiu, H. *et al.* ADR3, a next generation i-body to human RANKL, inhibits osteoclast formation and bone resorption. *Journal of Biological Chemistry*, 102889 (2023). https://doi.org:https://doi.org/10.1016/j.jbc.2023.102889

28 Drew, D. R. *et al.* Defining the Antigenic Diversity of Plasmodium falciparum Apical Membrane Antigen 1 and the Requirements for a Multi-Allele Vaccine against Malaria. *PLOS ONE* **7**, e51023 (2012). https://doi.org:10.1371/journal.pone.0051023

29 Vulliez-Le Normand, B. *et al.* Structural and Functional Insights into the Malaria Parasite Moving Junction Complex. *PLOS Pathogens* **8**, e1002755 (2012). https://doi.org:10.1371/journal.ppat.1002755

30 Lim, S. S. *et al.* Structure and Dynamics of Apical Membrane Antigen 1 from Plasmodium falciparum FVO. *Biochemistry* **53**, 7310-7320 (2014). https://doi.org:10.1021/bi5012089

31 Vulliez-Le Normand, B., Saul, F. A., Hoos, S., Faber, B. W. & Bentley, G. A. Cross-reactivity between apical membrane antgen 1 and rhoptry neck protein 2 in P. vivax and P. falciparum: A structural and binding study. *PLOS ONE* **12**, e0183198 (2017). https://doi.org:10.1371/journal.pone.0183198

32 Henderson, K. A. *et al.* Structure of an IgNAR-AMA1 complex: targeting a conserved hydrophobic cleft broadens malarial strain recognition. *Structure* **15**, 1452-1466 (2007). https://doi.org:10.1016/j.str.2007.09.011

33 Seidel-Greven, M. *et al.* Isolation and light chain shuffling of a Plasmodium falciparum AMA1-specific human monoclonal antibody with growth inhibitory activity. *Malaria Journal* **20**, 37 (2021). https://doi.org:10.1186/s12936-020-03548-3

34 Maskus, D. J. *et al.* Characterization of a novel inhibitory human monoclonal antibody directed against Plasmodium falciparum Apical Membrane Antigen 1. *Scientific Reports* **6**, 39462 (2016). https://doi.org:10.1038/srep39462

35 Silvie, O. *et al.* A Role for Apical Membrane Antigen 1 during Invasion of Hepatocytes by Plasmodium falciparum Sporozoites*. *Journal of Biological Chemistry* **279**, 9490-9496 (2004). https://doi.org:https://doi.org/10.1074/jbc.M311331200

36 Crewther, P. E., Matthew, M. L., Flegg, R. H. & Anders, R. F. Protective immune responses to apical membrane antigen 1 of Plasmodium chabaudi involve recognition of strain-specific epitopes. *Infect Immun* **64**, 3310-3317 (1996). https://doi.org:doi:10.1128/iai.64.8.3310-3317.1996

37 Dicko, A. *et al.* Impact of a Plasmodium falciparum AMA1 Vaccine on Antibody Responses in Adult Malians. *PLOS ONE* **2**, e1045 (2007). https://doi.org:10.1371/journal.pone.0001045

38 Ouattara, A. *et al.* Lack of allele-specific efficacy of a bivalent AMA1 malaria vaccine. *Malaria Journal* **9**, 175 (2010). https://doi.org:10.1186/1475-2875-9-175

39 Henry, K. A. & MacKenzie, C. R. Antigen recognition by single-domain antibodies: structural latitudes and constraints. *MAbs* **10**, 815-826 (2018). https://doi.org:10.1080/19420862.2018.1489633

40 Drew, D. R. *et al.* Defining species-specific and conserved interactions of apical membrane protein 1 during erythrocyte invasion in malaria to inform multi-species vaccines. *Cellular and Molecular Life Sciences* **80**, 74 (2023). https://doi.org:10.1007/s00018-023-04712-z

41 Scally, S. W. *et al.* PCRCR complex is essential for invasion of human erythrocytes by Plasmodium falciparum. *Nature Microbiology* **7**, 2039-2053 (2022). https://doi.org:10.1038/s41564-022-01261-2

42 Woehlbier, U., Epp, C., Hackett, F., Blackman, M. J. & Bujard, H. Antibodies against multiple merozoite surface antigens of the human malaria parasite Plasmodium falciparum inhibit parasite maturation and red blood cell invasion. *Malaria Journal* **9**, 77 (2010). https://doi.org:10.1186/1475-2875-9-77

43 Stanisic, D. I. & Good, M. F. Malaria Vaccines: Progress to Date. *BioDrugs* **37**, 737-756 (2023). https://doi.org:10.1007/s40259-023-00623-4

44 Devi, S. 12 countries to get first doses of malaria vaccine. *The Lancet* **402**, 172 (2023). https://doi.org:10.1016/S0140-6736(23)01456-3

45 Datoo, M. S. *et al.* Efficacy and immunogenicity of R21/Matrix-M vaccine against clinical malaria after 2 years' follow-up in children in Burkina Faso: a phase 1/2b randomised controlled trial. *The Lancet Infectious Diseases* **22**, 1728-1736 (2022). https://doi.org:10.1016/S1473-3099(22)00442-X

46 Adepoju, P. RTS,S malaria vaccine pilots in three African countries. *The Lancet* **393**, 1685 (2019). https://doi.org:10.1016/S0140-6736(19)30937-7

47 Srinivasan, P. *et al.* Immunization with a functional protein complex required for erythrocyte invasion protects against lethal malaria. *Proceedings of the National Academy of Sciences* **111**, 10311-10316 (2014). https://doi.org:doi:10.1073/pnas.1409928111

48 Patel, P. N. *et al.* Structure-based design of a strain transcending AMA1-RON2L malaria vaccine. *Nature Communications* **14**, 5345 (2023). https://doi.org:10.1038/s41467-023-40878-7

49 Yanik, S. *et al.* Structure guided mimicry of an essential P. falciparum receptor-ligand complex enhances cross neutralizing antibodies. *Nature Communications* **14**, 5879 (2023). https://doi.org:10.1038/s41467-023-41636-5

50 Patel, P. N. *et al.* Neutralizing and interfering human antibodies define the structural and mechanistic basis for antigenic diversion. *Nature Communications* **13**, 5888 (2022). https://doi.org:10.1038/s41467-022-33336-3

51 Kisalu, N. K. *et al.* A human monoclonal antibody prevents malaria infection by targeting a new site of vulnerability on the parasite. *Nature Medicine* **24**, 408-416 (2018). https://doi.org:10.1038/nm.4512

52 Kayentao, K. *et al.* Safety and Efficacy of a Monoclonal Antibody against Malaria in Mali. *New England Journal of Medicine* **387**, 1833-1842 (2022). https://doi.org:10.1056/NEJMoa2206966

53 Gaudinski, M. R. *et al.* A Monoclonal Antibody for Malaria Prevention. *New England Journal of Medicine* **385**, 803-814 (2021). https://doi.org:10.1056/NEJMoa2034031

54 Wu, R. L. *et al.* Low-Dose Subcutaneous or Intravenous Monoclonal Antibody to Prevent Malaria. *New England Journal of Medicine* **387**, 397-407 (2022). https://doi.org:10.1056/NEJMoa2203067

55 Chandley, P., Ranjan, R., Kumar, S. & Rohatgi, S. Host-parasite interactions during Plasmodium infection: Implications for immunotherapies. *Frontiers in Immunology* **13** (2023). https://doi.org:10.3389/fimmu.2022.1091961

56 Trager, W. & Jensen, J. B. Continuous culture of Plasmodium falciparum: its impact on malaria research. *International Journal for Parasitology* **27**, 989-1006 (1997). https://doi.org:https://doi.org/10.1016/S0020-7519(97)00080-5

57 Moon, R. W. *et al.* Adaptation of the genetically tractable malaria pathogen Plasmodium knowlesi to continuous culture in human erythrocytes. *Proceedings of the National Academy of Sciences* **110**, 531-536 (2013). https://doi.org:doi:10.1073/pnas.1216457110

58 Chatzileontiadou, D. S. M., Szeto, C., Jayasinghe, D. & Gras, S. Protein purification and crystallization of HLA-A∗02:01 in complex with SARS-CoV-2 peptides. *STAR Protocols* **2**, 100635 (2021). https://doi.org:https://doi.org/10.1016/j.xpro.2021.100635

59 Minsky, A., Summers, R. G. & Knowles, J. R. Secretion of beta-lactamase into the periplasm of Escherichia coli: evidence for a distinct release step associated with a conformational change. *Proceedings of the National Academy of Sciences* **83**, 4180-4184 (1986). https://doi.org:doi:10.1073/pnas.83.12.4180

60 Schrodinger, L. The PyMOL Molecular Graphics System (2015).

61 Persson, K. E. M., Lee, C. T., Marsh, K. & Beeson, J. G. Development and Optimization of High-Throughput Methods To Measure Plasmodium falciparum-Specific Growth Inhibitory Antibodies. *Journal of Clinical Microbiology* **44**, 1665-1673 (2006). https://doi.org:doi:10.1128/jcm.44.5.1665-1673.2006

62 Hadley Wickham. *ggplot2: Elegant Graphics for Data Analysis*. (Springer-Verlag New York, 2016).

63 R: A Language and Environment for Statistical Computing (R Foundation for Statistical Computing, Vienna, Austria, 2023).

64 Ritz, C., Baty, F., Streibig, J. C. & Gerhard, D. Dose-Response Analysis Using R. *PLOS ONE* **10**, e0146021 (2016). https://doi.org:10.1371/journal.pone.0146021

65 Drew, D. R. *et al.* Functional Conservation of the AMA1 Host-Cell Invasion Ligand Between P. falciparum and P. vivax: A Novel Platform to Accelerate Vaccine and Drug Development. *J Infect Dis* **217**, 498-507 (2018). https://doi.org:10.1093/infdis/jix583

Supplementary Files

This is a list of supplementary files associated with this preprint. Click to download.

- ExtendedData1.pdf
- ExtendedDataSheet1.xlsx